PONTIFICIA UNIVERSIDAD CATOLICA DE CHILE
ESCUELA DE INGENIERIA

TOWARDS DIRECT METAL LASER FABRICATION OF CU-AL-NI SHAPE MEMORY ALLOYS

GONZALO SEBASTIÁN REYES DONOSO

Thesis submitted to the Office of Research and Graduate Studies in partial fulfillment of the requirements for the Degree of Master of Science in Engineering

Advisor:
MAGDALENA WALCZAK

Santiago de Chile, August 2015

PONTIFICIA UNIVERSIDAD CATOLICA DE CHILE
ESCUELA DE INGENIERIA

TOWARDS DIRECT METAL LASER FABRICATION OF CU-AL-NI SHAPE MEMORY ALLOYS

GONZALO SEBASTIÁN REYES DONOSO

Members of the Committee:

MAGDALENA WALCZAK

JORGE RAMOS GREZ

ESTEBAN RAMOS MOORE

DIEGO LÓPEZ-GARCÍA GONZÁLEZ

Thesis submitted to the Office of Research and Graduate Studies in partial fulfillment of the requirements for the Degree of Master of Science in Engineering

Santiago de Chile, August 2015

To God, my Parents, siblings, fiancée and friends, who supported me and gave me the strength to accomplish this dream.

ACKNOWLEDGMENTS

Firstly, I am grateful to God for the good health and wellbeing that were necessary to complete this master and mechanical engineer degree.

I must express my deepest gratitude to Professors Magdalena Walczak and Jorge Ramos for their advice, support and guidance throughout this thesis. This master thesis has been a very difficult path, especially in one moment when everything seemed to be lost and I would never be able to finish it without them.

My sincere thanks also goes to Professor Esteban Ramos Moore, for his willing to help and advise me with the vacuum technology management among other necessary knowledge for my experiments. Also thank my fellow labmates Rodrigo del Pozo, Alan Valenzuela, Hongping Mei and Gabriela Bravo for their help in the different stages of the experimental set-up needed for this work.

I want to specially thank my fiancée Daniela Faúndez for hear me, hold me and support me with her love through this long period. Also, I appreciate María Donoso's spiritual guidance and support while walking this path.

I take this opportunity to express gratitude to all the members of the mechanical department for their help and support: Luis Valdés, Marcelo, Nacho, Roberto, Fabián, Parra, Enrique, Miguel Ángel, Gloria, Anita, Alejandra, Patricio Pérez and Manuel Galvez.

Special thanks to my friends, who played a key role throughout all this years and especially to my roommates for their support during this last time.

I also thank the financial support of the Chilean Council of Research and Technology, CONICYT through their FONDECYT Project No.1130906.

Finally, I would like to express my sincere gratitude to my parents Víctor and Eliana, and my dear siblings Víctor Hugo and Carolina; to them and their constant affection, support, patience and effort, I owe everything I am and will be.

TABLE OF CONTENTS

LIST OF TABLES

LIST OF FIGURES

ABSTRACT

This work is motivated by the search for materials alternative to the Ni-Ti shape memory alloy (SMA) that would provide similar shape memory properties but at the lower cost of the base material. In this context, three Cu–Al–Ni alloys are selected to verify the applicability of direct metal laser fabrication process (DMLF) for the fabrication of shape memory alloys. The method consists in laser melting of metallic powder precursors in a controlled atmosphere. The effect of Al content, laser power, and laser exposure time are studied. In all the obtained materials, microstructures and phase change transformation temperatures typical for Cu-based SMA were found. The increase in laser power and prolonged laser exposure time were found to be associated with the formation of γ2 phase and thus unfavorable for the SMA microstructure. The effect is enhanced in the case of higher Al-content. The results serve as a proof of concept for further development of DMLF-based additive manufacturing of Cu-based shape memory alloys.

Keywords: Shape memory alloys, SMA, direct metal laser fabrication, DMLF, Cu-Al-Ni alloy, austenitic transformation.

RESUMEN

Este trabajo es impulsado por la búsqueda de materiales alternativos a las aleaciones de Ni-Ti con memoria de forma (SMA) que puedan ofrecer propiedades similares pero a un menor costo de materias primas. En este contexto se seleccionaron tres aleaciones de Cu–Al–Ni para probar la aplicabilidad del método de fabricación directa de metal asistida por láser (DMLF) para producir aleaciones con memoria de forma. Él método consistió en la fundición de polvos metálicos en una atmósfera controlada. Fueron estudiados los efectos de la concentración de Al, potencia del láser y tiempo de exposición de láser. En todas las muestras obtenidas se encontraron microestructuras y temperaturas de transformación de fase típicas de aleaciones con memoria de forma basadas en Cu. Además, se descubrió que el aumento de la potencia del láser y la prolongación del tiempo de exposición láser están asociados a la formación de fases γ_2, las cuales no favorecen la microestructura de una aleación con memoria de forma. El efecto es potenciado cuando hay mayores concentraciones de Al. Los resultados de este trabajo podrían servir cómo una prueba del concepto propuesto, útiles para el futuro desarrollo de métodos basados en DMLF de manufactura aditiva de aleaciones con memoria de forma basadas en Cu.

Keywords: Aleaciones con memoria de forma, SMA, fabricación asistida con láser, DMLF, Cu-Al-Ni, transformaciones martensíticas.

1. SCIENTIFIC BACKGROUND

1.1. Introduction

The shape memory effect (SME) is a property that some materials have, which makes them capable to return to their original shape after being deformed. The metallic alloy, which have SME are called shape memory alloys (SMA) and the SME is driven by a phase change known as a thermoelastic martensitic transformation. The low and the high temperature phases are called by analogy to the steel technology as martensitic and austenitic temperatures. This phase change allows these materials to recover their original shape after being heated up until their critical transformation temperature. Also, above the transformation temperature some of them exhibit an unusual large strain deformation in an elastic range called pseudoelasticity. Some authors precise that pseudoelasticity corresponds to any apparently elastic deformation that can disappear after unloading the material, and that super elasticity correspond to a pseudoelasticty which involves a stress trigged transformation from austenite to martensite. So, the term pseudoelasticiy includes the superelasticity (Lojen et al., 2005).

Due their potential uses to generate motion or force with the shape memory effect and store energy with their superelasticity properties, the SMAs have been widely studied in order to use them in several fields. For example, there are several studies related to damping systems (Jiao et al., 2010) use the superelasticity effect in high temperature condition (austenite phase) for earthquake damping or, in other cases; using the internal friction at low temperature condition (in martenstitic phase) suitable for passive damping (Humbeeck, 2001). However, in general terms, these properties are observed just in micro scale and they not necessary exhibit a good behavior at macroscopic scale. In order to solve this issues it is also possible to generate crystallographic textures which allows to add the contribution of each grain of material in micro scale to produce a desirable behavior in the material at macroscopic scale (Sobrero et al., 2012).

This work is the first of several studies that seek to create crystallographic textures in selected Cu-based alloys to maximize the superelasticity property using the *direct metal*

laser fabrication (DMLF) method. There are other studies that seek to obtain crystallographic textures in Cu-based alloys (Lojen et al., 2005, 2013; Motoyasu et al., 2001), but none of them had used a laser sintering method.

The DMLF process was developed in the mid-90s by the creators of a similar method called *selective laser sintering* SLS™(Deckard, 1989). Both technologies rely on a laser guided material transformation, but the SLS™ is focused on fabrication of complex geometry objects with a sintering process (forming a solid structure from powders without melting). In contrast, the DMLF uses a powder metal melting process to obtain the desired solid structure. However, neither of them have been used to fabricate Cu–based shape memory alloys; yet there are few research which are focused on Ni–Ti based SMAs (Halani & Shin, 2011; Kyogoku et al., 2003). This work seeks to initiate a path of DMLF methods applied to Cu-based SMAs, studying the behavior of a Cu–Al–Ni alloy due their potentially good strain recovery. The main issue of this alloy is the brittleness that presents due their anisotropy, which is expected to be resolved with a specific laser fabrication in advanced stages of this work.

The rest of this chapter is structured as follows: section 1.2 states the main objectives pursued in this work, section 1.3 presents a literature review of the main theoretical framework about the shape memory effect in metallic alloys, some main characteristics of Cu–based shape memory alloys and a brief description of the direct metal laser method. Section 1.4 exposes the main conclusions of the present research, and section 1.5 describes the difficulties faced by the proposed fabrication method and possible paths and recommendation for future research. Following this, chapter 2 contains the main article of this thesis. Within this, section 2.1 presents a brief introduction of the article, section 2.2 introduces the experimental set-up and methodologies used, section 2.3 present the main obtained results, section 0 presents the reported results discussion and finally section 2.5 presents the conclusions that can be drawn. More, details about the initial state of the metallic powders, specific values obtained at DSC and their respective curves are presented in the appendix.

1.2. Main objectives

The aim of this work is to develop a laser melting method for Cu–based SMAs fabrication, starting a path of research that seeks to find an additive manufacturing method to fabricate functional Cu–based SMA with controlled microstructure to be suitable for damping applications.

To achieve the global objective, this work proposes that it is possible to fabricate Cu–Al–Ni SMAs from metal powder by a laser melting process. In order to prove that, this work carries three specific objectives:

1. The first one is to build an experimental set-up capable to control atmosphere parameters (to avoid excess of oxygen) and apply a laser beam controlling time of application and power on elementary mixed powders in order to obtain a Cu–Al–Ni alloy.
2. The second objective is to study the behavior of Cu–Al–Ni alloys fabricated by a laser melting method varying the Al content and laser parameters reporting the sensitivity of the system to those changes.
3. Finally, the third objective is to find at least one combination of laser power, time of laser exposure and Al content capable to produce a Cu–Al–Ni alloy with fully martensitic microstructure that exhibits some SMAs characteristics without the necessity of any post thermal treatment.

1.3. Literature review

1.3.1. Shape memory effect and superelasticity phenomenon

Despite this effect was discovered in 1932 by Arne Ölander (Ölander, 1932), it was used for the first time in 1945 by Vernon (Vernon & Vernon, 1941). However, the shape memory materials became a relevant field of study when William Buehler and Frederick Wang showed the shape memory effect (SME) was present in a Nickel-Titanium alloy in 1962 (Buehler et al., 1963; Kauffman & Mayo, 1997), also better known as Nitinol

(from the combination between the elementary components and “Naval Ordnance Laboratory”, the place where the alloy was discovered). From that moment the SMAs have been used for several applications in automobile, aeronautics, medicine among others industries as a finished products or as a prototype (Mohd Jani et al., 2014).

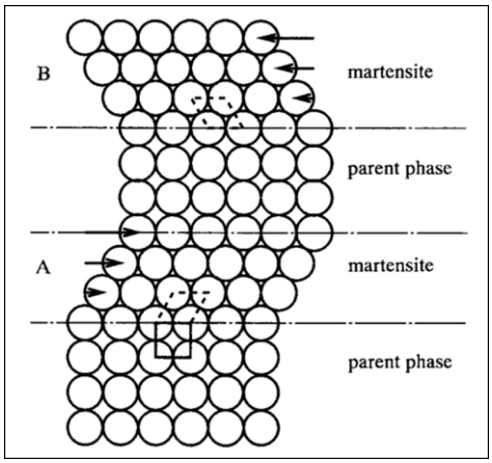

Fig. 1: A simplified model of martensitic transformation (Otsuka & Wayman, 1999).

The SME is a unique property that some materials exhibit. In metallic alloys this is caused by martensitic transformations driven by a difussionless phase change due a cooperative movement of atoms which act as if a shear stress was applied, involving a lattice distortion which leads macroscopic shape changes (Van Humbeeck, 2001). The temperatures which induces phase changes in this alloys are usually characterized as A_s and A_f (austenitic transformation start and finish temperatures) a during heating and Ms and M_f (martensitic transformation start and finish temperatures) during cooling. When the temperature cools down from the high temperature stable phase (parent phase called austenitic phase) it transforms martenstically (starting at a temperature below M_s and finishing when it reaches the M_f temperature) as its exemplified in Fig. 1 scheme, where when the temperature is lowered the parent phase changes into different martensite variants (A and B) due shear-like mechanism. However, during the nucleation and growth process, two mechanisms of lattice invariant shear can occur to reduce the strains

generated by this phase transformation, which are the introduction of a slip (b) or an introduction of twins (c) as it is schematically represented in Fig. 2. The specific mechanism depends on the specific alloy used but the twinning is usually present in SMAs. The twins can also acts in a deformation mode under stress creating a macroscopic shape change, which is reversible when the material is heated above the A_f temperature recovering the parent phase with its macroscopic original shape.

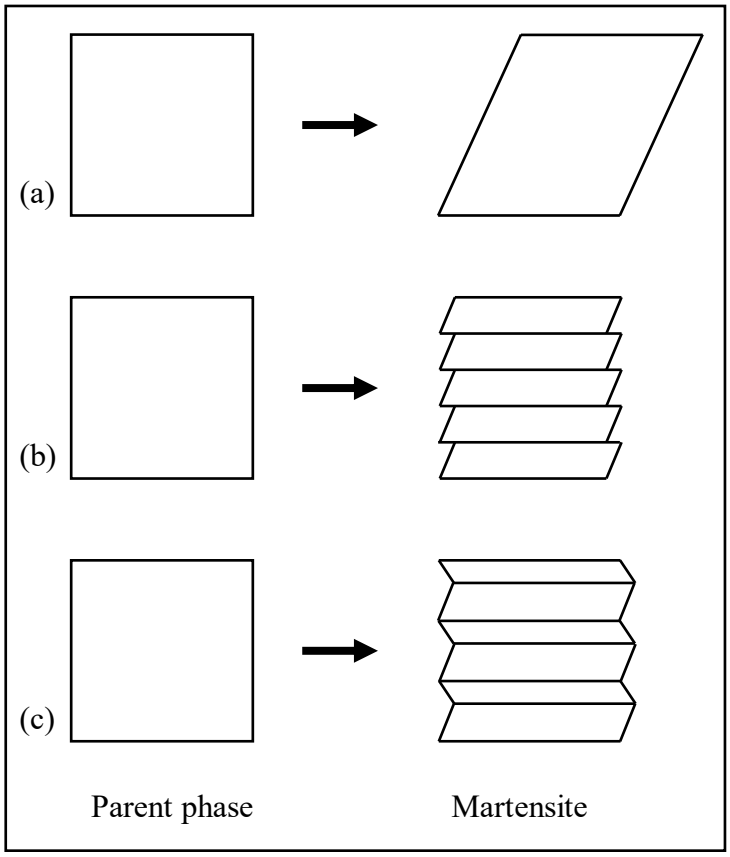

Fig. 2: Schematically shows why the lattice invariant shear is required upon martensitc transformation; (a) shape change upon martensitic transformation; (b) and (c) represent the accommodation of strain by introducing slip (b) or twins (c) respectively (Miyazaki & Otsuka, 1989).

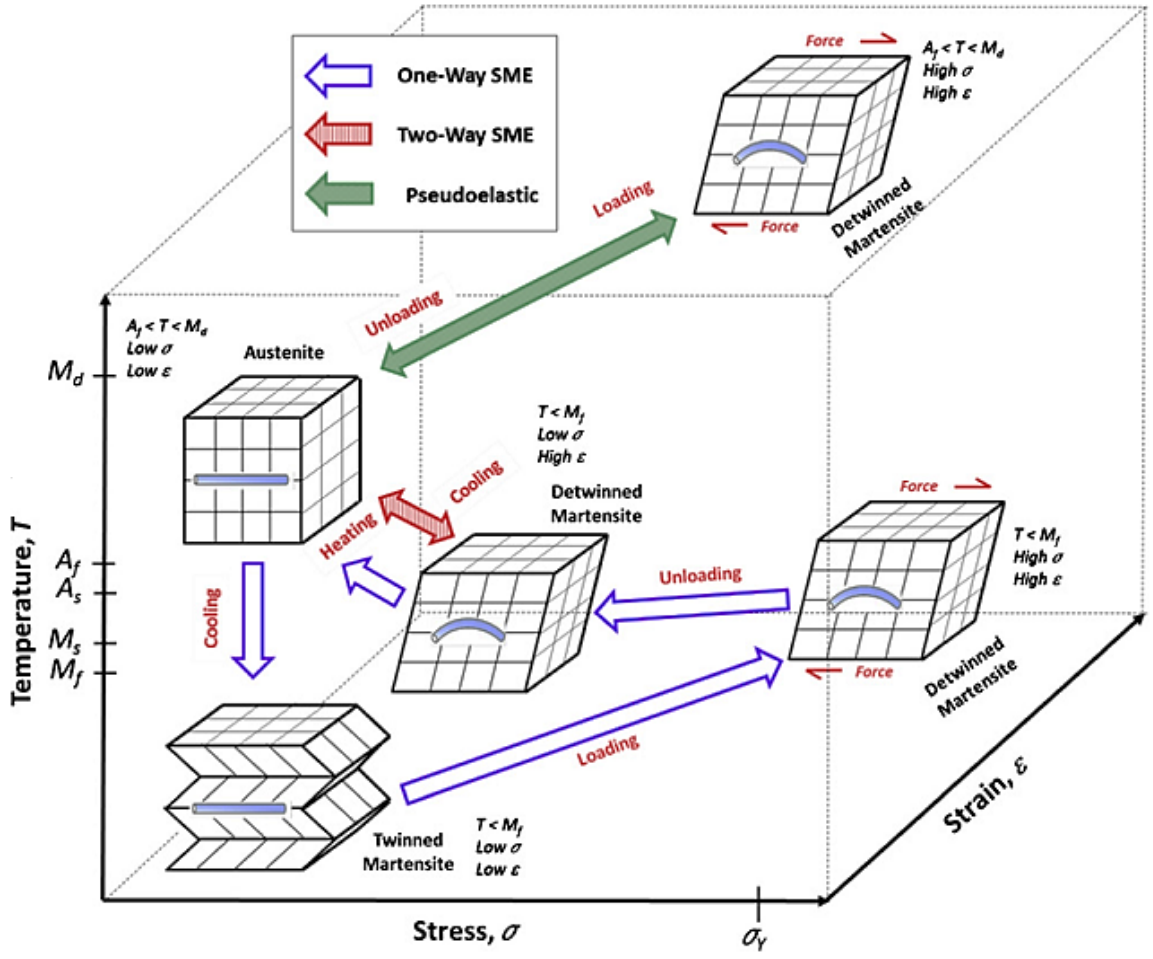

Fig. 3: SMA phases and their crystal structures (Mohd Jani et al., 2014).

There are three main shape memory characteristics that can be associated with the SMAs (schematically illustrated in Fig. 3.). The first one relies in the property of the alloy to almost full recover its original shape ("hot shape") after being deformed to almost every shape (without exceeding a certain strain limit which is at about 8% in the best cases) which is called One Way Shape Memory Effect (OWSME). In addition to OWSME the second characteristic is known as Two Way Shape Memory Effect (TWSM) which consists in the capacity of the material to also "remember" a cold temperature shape but it has to be thermally trained to obtain that capacity and usually produces about half of the recovery strain than a same alloy, which presents only OWSME. Finally the third

characteristic called superplasticity is the capacity the alloy to admit unusual large reverse strains when is loaded at temperatures above A_f because under those conditions the martensitic phase change is induced by high stress levels but when the material is unloaded it immediately starts a reverse transformation to austenitic phase which is the stable phase at that temperature.

1.3.2. Cu-based shape memory alloys (SMAs)

There are several studies about Cu-based SMAs due their potentially uses in damping systems, good strain recovery, fabrication costs and their thermal stability at high temperatures (Van Humbeeck et al., 1993). Typically the specific properties of the Cu-based SMAs relies in the alloying components, for example, Cu-Zn-Al alloys exhibit good ductility and reproducibility but they have a poor stability in temperatures above 200°C, in contrast to the Cu-Al-Ni which has an excellent high temperature stability above 200°C, but lacks a good reproducibility (Van Humbeeck et al., 1993).

Typically in Cu-based alloys are three important phases: Cu primary FCC precipitates recognized as α phases, a high temperature stable phase (austenite) known as β phase, and typically a martensite phase. In Cu–Al–Ni alloys the high temperature stable and disordered β phase is known as β_3, which undergoes a eutectoid decomposition at lower temperatures into α (primary solid solution of Cu FCC) and γ_2 (Cu_9Al_4 cubic face), but if it is quenched in β_3, it transforms martensically into β'_3 or γ'_3, depending on the cooling rates and in the specific proportion of the alloying elements. As it is remarked in the main article of this present work, historically, the parent phase β and martensite phases β' and γ' usually have been labeled with a subindex 1 according to the martensites nomenclature, because they were recognized with a DO_3 ordering which is the nearest next neighbor order, but according to Recarte et al. (2002) observations based on Delaey & Chandrasekaran (1994) comments, they actually has a $L2_1$ order. In consequence they should be labeled with a subindex 3 according to martensites nomenclature, but it is very common to find studies which uses any of both subindex.

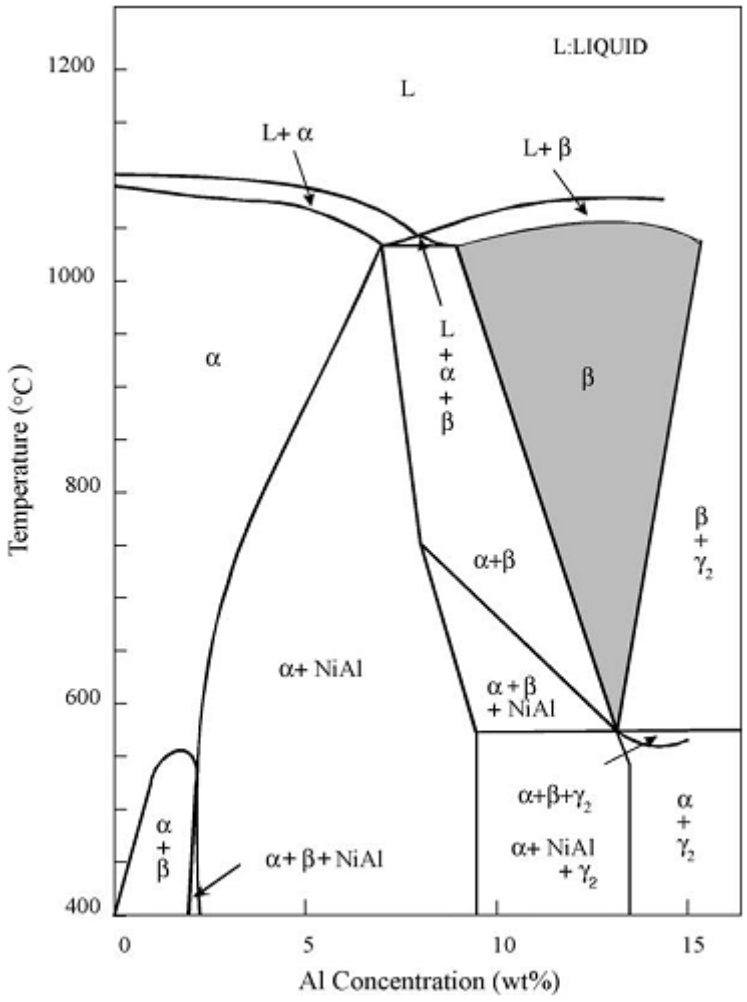

Fig. 4: Ternary phase diagram Cu–Al–Ni, vertical cross-section at 3 wt. % Ni (Lojen et al., 2005).

Cu-Al-Ni alloys are very sensitive to the proportion of their alloying components, fabrication process and thermal treatments. Changes in the proportion of the composition elements can drastically change the transformation temperatures and the martensites obtained at low temperature (Otsuka et al., 1999; Recarte et al., 2002). In other hand the cooling rates are very important because they also affects the precipitation of γ_2 (Dagdelen et al., 2003; Lojen et al., 2005, 2013; Otsuka et al., 1999; Recarte & Pérez-Sáez, 1997). A more detailed description about the sensitivity of Cu-Al-Ni alloys to the mentioned parameters is going to be given in the main article.

1.3.3. Direct metal laser fabrication (DMLF) process

The Direct metal laser fabrication process consists of a melting mechanism of metal powder assisted by laser. It was developed with the objective to directly process metals in freeform producing fully dense components with mechanical properties comparable to those of materials classically processed in short times. (Gu et al., 2012). This rapid prototyping process is a powder bed fusion process, where the entire zone which is affected by the laser is melted during a first scan, and in the subsequent scans a portion of the previously solidified material is re-melted creating a well-bonded, high density structure (Gibson et al., 2009). However, the resulting pieces are affected by several parameters which can be classified in four categories: laser parameters (laser power, spot size, pulse duration, pulse frequency, angle of incidence, among others), powder parameters (particle size, shape, and distribution, layer thickness, material properties, etc.), scan speed parameters (scan speed, spacing and pattern) and the temperature related parameters (powder bed temperature, powder feeder temperature, temperature uniformity, etc.) (Gibson et al., 2009). For instance, the laser wavelength will affect the energy absorption of the metal powders, being more efficient to use an Nd-YAG laser than a CO_2 laser to melt metal powders (Gibson et al., 2009). Moreover, these parameters are usually interrelated, for example, the powder shape and size of the powders also affects the laser absorption characteristics, powder bed density, thermal conductivity and powder spreading. Usually finer powders particles provide greater surface area, and absorbs energy more efficiently (Gibson et al., 2009). However, some combinations of laser parameters and material properties can cause the balling phenomenon (Gu & Shen, 2007, 2009; Gu, 2015; Kruth et al., 2004), which involves a diminishing in the surface energy of liquid reaching final equilibrium state of several metallic agglomerates with spherical shape during laser melting along a row of powder particles (Gu, 2015). This is a complex metallurgical phenomenon, which presents

different kinds of working mechanism in some metallic alloys, and can be controlled by both powder material properties and the laser processing conditions.

1.4. Main Conclusions

The particular characteristics of SMAs and its potential applications has led researchers to seek for a better understanding of its properties and suitable manufacturing methods. In spite of this, only few studies had explored the suitability of additive manufacturing methods for SMAs fabrication, and to our best knowledge, there are no reports of a DMLF or any laser assisted additive manufacturing method used in Cu-based SMAs. This thesis proposes a laser assisted fabrication method of Cu-Al-Ni SMAs, which consists in a DMLF like method but focused on only one melting point. This is done to study the obtained properties of the fabricated alloy, concluding that this is a suitable manufacturing method for Cu–Al–Ni alloys fabrication from elementary powders mixture.

The fabricated alloys present typical SMA properties such as the microstructure, DSC curves and hysteresis values in the stress-strain-temperature diagram. The specimens exhibit a γ_2 precipitation increase when any of the experimental parameters (time of laser exposure, laser power and Al content) was increased. However, there is a combined effect of these parameters when all of them are set at their higher values. The hardness values obtained using this experimental set-up are controlled mainly by the precipitation of γ_2 phases. Also there was a great increment of γ_2 precipitation when the experimental parameters were set at the most highest values, confirming the idea of the existence of a combined effect. On the other hand, the hysteresis of the phase transformation is mainly driven by the Al content, rather than the other experimental parameters used in this experimental set-up.

1.5. Further Research

It is important to notice that the mixing process used for this work was enough to study the suitability of a laser melting method for Cu-based SMA fabrication. In spite of that, it is very likely that improving the mixing process would improve the precision in the composition of the fabricated specimens, and also should improve the performance of the material properties. However, should the evaporation of persist (affecting the composition), an experimental set-up to vary the argon pressure (Masmoudi et al., 2015) might prove necessary. Given the effectiveness of the proposed methodology, this research could be continued by studying several scan patterns to obtain a microstructural texture, in order to exhibit the material anisotropy as a macroscopic property of the fabricated specimens, improving the mechanical properties. On the other hand, if it is desired to use this Cu-based alloy and method for seismic damping, it should be consider to increase the Ni content to 4 wt.% and, if it is necessary, also an Al content increase or even a combination with Mn to lower the transformation temperatures in order to obtain super elasticity properties at room temperature.

Finally, an important issue that it has to be attended is the balling phenomenon, which was present in the preliminary tests performed using this experimental set-up. This is a common phenomenon present in direct laser melting processes (Gu et al., 2007, 2009; Kruth et al., 2004), but it can be controlled varying the scanning rate, the thickness of the applied powder bed, the initial temperature of the process, the laser power and spot size among others.

2. MAIN ARTICLE: TOWARDS DIRECT METAL LASER FABRICATION OF CU–AL–NI SHAPE MEMORY ALLOYS

2.1. Introduction

Various techniques of additive manufacturing of metallic alloys have been extensively studied as an alternative for rapid fabrication of functional prototypes and tools (Gibson et al., 2009); among them, selective laser sintering (SLS™) and direct metal laser fabrication (DMLF). Both techniques exploit the possibility of inducing phase transformation, mostly solid-liquid-solid, by interaction with a laser beam. The SLS™ is focused on fabrication of complex geometry objects through the sintering process, forming a solid structure from powders without complete melting. In contrast, the DMLF uses a powder metal melting process to obtain the desired solid structure, producing fully dense components with mechanical properties comparable with materials manufactured by traditional methods, but in shorter times. However, only a few studies have explored the suitability of laser based additive manufacturing for fabricating shape memory alloys like Ni–Ti.

The shape memory alloys (SMAs) are metallic alloys capable of returning to their original shape after being deformed owing to a phase transformation known as a thermoelastic martensitic transformation, termed so in analogy to steel technology. Some of the alloys are additionally attractive for the superelasticity effect permitting dissipation and storage of energy (Liu et al., 2015). This property is of particular interest for systems of mechanical damping (Jiao et al., 2010). The practical uses of SMAs as prototypes or even finished products have been reported in industries such as automobile, aeronautics and biomedical (Mohd Jani et al., 2014).

The most studied SMA is Nitinol (Ni–Ti), allowing for the highest known working stresses and recoverable strains, as well as highest stability in cyclic applications (Humbeeck, 2001). Cu–based SMA alloys are considered a lower cost alternative that might lead to engineering applications of larger volume (Otsuka et al., 1999). Among the Cu–based SMA, Cu–Al–Ni are attractive due to their thermal stability at high

temperature (Miyazaki et al., 1989). Cu–Al–Ni alloys has a stable high temperature and disordered β phase which undergoes an eutectoid decomposition at lower temperatures into α phase (primary solid solution of Cu) and γ_2 phase (Cu_9Al_4 cubic face), but if it is quenched from β phase it transforms martensically (Otsuka et al., 1999). Typically the martensitic β' phases of this alloy are labeled with a subindex 1, however as Recarte et al. (2002) used in their research based on Delaey and Chandrasekaran (1994) observations, they should be labeled according to the martensitic nomenclature with a subindex 3 because of their $L2_1$ order. At low temperature, the thermally induced martensites phases evolves from β'_3 (18R) to γ'_3 (2H) depending on the Al content (Recarte et al., 2002). On the other hand, the low cooling rates and especially high Al content also causes the precipitation of γ_2 phases, which in some cases are not avoided by quenching (Miyazaki et al., 1989). The transformation temperatures of this alloy are sensitive to thermal treatments (Dagdelen et al., 2003) and cooling rates during the fabrication, showing important changes (Lojen et al., 2013).

The only available works on direct metal laser fabrication of SMAs have been reported on Ni–Ti alloys. Halani and Shin (2011) characterized a Nitinol alloy fabricated by direct laser deposition, whereas Kyogoku et al. (2003) studied the applicability of laser melting for fabrication of Ni-Ti and Shishkovsky (2005) used an SLS approach to fabricate porous volume Ni-Ti. However, to our best knowledge, no attempt of producing Cu-based SMA by direct metal laser fabrication (DMLF) has been reported so far. The aim of this work is to explore the suitability of laser melting methods for fabrication of Cu–Al–Ni alloys with martensitic microstructure in the context of possible further development towards an additive manufacturing method. Considering the capacity of laser to control microstructure, in particular producing columnar grains, would allow fabrication of large pieces which is currently possible only through directional solidification – a method shown to be effective for improving shape memory characteristics of Cu-based SMA (Yuan et al., 2015). With this motivation, the effects of time laser exposure, power of laser application, and Al content variations in the fabrication of Cu–Al–Ni alloys are analyzed.

2.2. Experimental

2.2.1. DMLF set-up

The set-up consisted on a vacuum heating system coupled with a laser source shown schematically in **Fig. 5**. Samples of elementary powder mixtures were mounted in ceramic crucibles on the top of a resistance heater inside the vacuum chamber. The surface of the samples were irradiated using an Ytterbium 1070 nm wavelength laser, model YLR-300-MM-AC-Y11 from IPG Photonics.The laser was controlled by a PC allowing accurate positioning (~1 mm) of the laser spot over the desired surface through copper mirrors actuated by stepper motors. This set-up allowed the fabrication of up to five specimens per experimental run. A pyrometer (Marathon MR from Raytek) mounted outside the vacuum chamber was used to measure the temperature of the samples during the experiment.

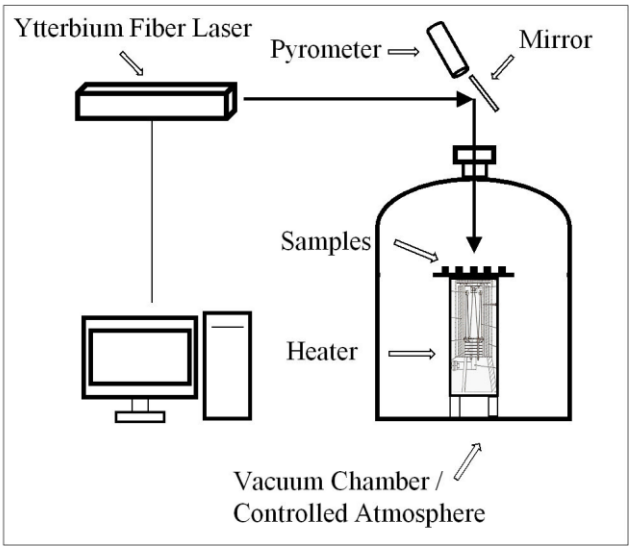

Fig. 5: Schematic view of the entire experimental set-up used for the alloy fabrication.

2.2.2. Fabrication procedure

The following metallic powders from Sigma Aldrich were used: Al min. 93% pure, Cu 99% pure and Ni 99.99% pure. The particle size of the powders was 5 μm (fine powder), 14-25 μm and 149 μm (mesh < 100), respectively. The elementary powders were weighed using an analytical balance and then mixed by manual maceration in 2 ml of ethanol for about 10 min until becoming a homogenous dough-like suspension of high density. The mass was then transferred to a ceramic crucible preconditioned in the vacuum system at 4 $\times 10^{-6}$ mbar and 400 °C for 20 hours. Then, the chamber was filled with argon at ~1 atm, and the samples irradiated using the laser parameters described in Table 1. The peak temperature occurred during the application of the laser and reached more than 1400 °C. Subsequently, the heater was then turned off and the chamber opened after three hours of natural cooling. The mass loss was determined by weighing the samples with crucibles before and after the process.

Three alloy compositions, two levels of laser power and three levels of laser application time were considered for designing the fabrication procedure. The obtained solid samples were labeled according to the composition, laser radiation exposure time, and output laser power. The intensity factor is a qualitative parameter that depends on the relative intensity of the key fabrication parameters: percentage of Al, laser power and laser exposure time.

Table 1: Description of the fabrication parameters.

Intensity Factor	Low	Medium	High
Composition	14.2 wt.% Al	14.8 wt.% Al	14.9 wt.% Al
Laser power	232 W	-	300 W
Exposure Time	0.3 s	0.5 s	1.0 s

2.2.3. Characterization

Low speed saw (Buehler IsoMet) was used to cut the samples. Differential scanning calorimetry (DSC) was performed in a rich Ni atmosphere using Perkin-Elmer DSC-6000 at the scanning rate of 10 $K \cdot min^{-1}$, in order to study the samples phase transformations. The samples were mechanically polished and etched by a solution of iron chloride (2.5 g $FeCl_3 \cdot 6H_2O$, 48 ml methanol, 10 ml HCl). The time of etching was 90 s for samples with low Al content (14.2 wt.%) and 60 s for the others. Optical imaging was performed using Nikon OPTIHOT-100 microscope and the images were digitalized by the Moticam 2300 system. Processing of the obtained images was completed using Image J (Abràmoff et al., 2004). Scanning electron microscopy (SEM) LEO 1420VP equipped with energy dispersive X-Ray analysis (EDX) from Oxford Instruments was used for imaging and elemental analyses. Both analyses were performed at 25kV of acceleration voltage. Finally, Vickers micro hardness was performed using the Leco M-400-H testing machine.

2.3. Results

2.3.1. Composition

The elemental compositions of the pre-treated and post-treated samples were obtained by weight and EDX analysis, respectively (**Table 2**). It is worth to note that the precision of the weight and EDX measurements were ~0.0001 wt. % and ~1 wt.%, respectively. The standard deviation of the EDX analyses was estimated after systematic measurements performed in 11 similar post-treated samples. The loss of mass associated with the heat and laser processing is shown in **Fig. 6**. All samples experienced reduction of mass, whereas higher Al content is generally associated with a higher mass loss, due to its low fusion point.

Table 2: Weight composition determined by weight and EDX analysis

	Low Level wt. % Al			Medium Level wt. % Al			High Level wt. % Al		
	Cu	**Al**	**Ni**	**Cu**	**Al**	**Ni**	**Cu**	**Al**	**Ni**
Pre-treated Weight Analysis	82.8	14.2	3.0	82.2	14.8	3.0	82.1	14.9	3.0
Post-treated EDX Analysis	83.2± 0.8	13.7± 0.8	3.1± 0.2	83.4± 0.5	13.5± 0.7	3.2± 0.2	82.3± 1.6	14.6± 1.8	3.1± 0.3

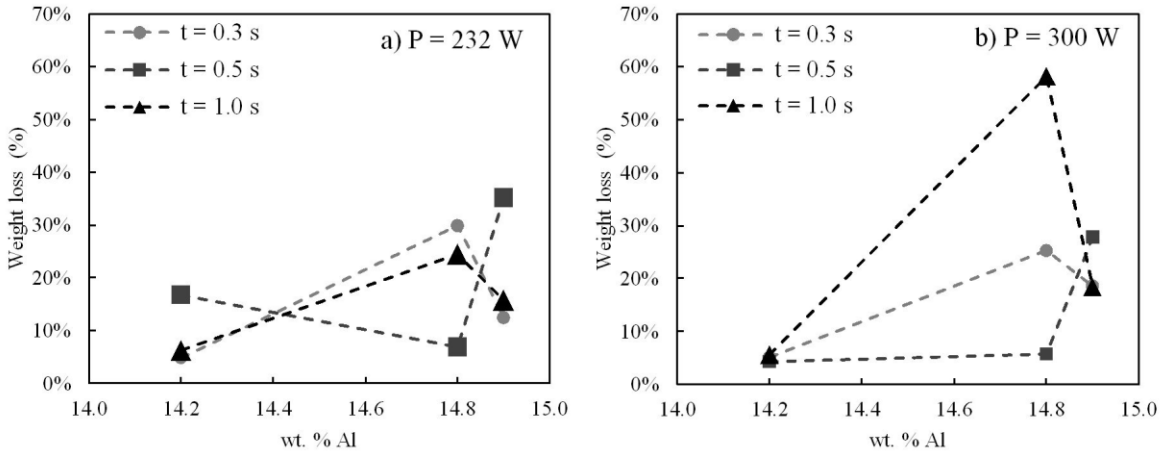

Fig. 6: Weight loss (in percentage) of samples fabricated (showed at their nominal wt.% Al composition) with an average peak temperature of 1410 °C.

2.3.2. Microstructure

Metallographic analysis reveals three types of microstructure shown in **Fig. 7**. The first type is fully martensitic with typical well-shaped needles exemplified in **Fig. 7**a, **Fig. 7**b, **Fig. 7**c and **Fig. 7**d with sparse black precipitations. The second type of microstructure includes star-like dendrites of relatively small size dispersed in thin martensitic structures exemplified in **Fig. 7**e and **Fig. 7**f. Finally, the third type of microstructure exemplified in **Fig. 7**g and **Fig. 7**h is characterized by larger and numerous dendrites. It should be noted, that two types of martensitic structures were observed: one with

irregular zig-zag morphology (**Fig. 7**a, **Fig. 7**b and **Fig. 7**c) and the other with parallel plates (**Fig. 7**d).

All of the three types of microstructures depend on the fabrication parameters. For instance, an increase in aluminum content generally results in the formation of more dendrites (**Fig. 8**). Whereas, samples with 14.2 wt.% Al tend producing thinner martensite structures at high laser power; and the time of laser exposure produces increased number of precipitates. A similar observation is made for samples with 14.8 wt.% and 14.9 wt.% of Al. They show an increase in the size and number of dendrites with the increase of laser power and exposure time.

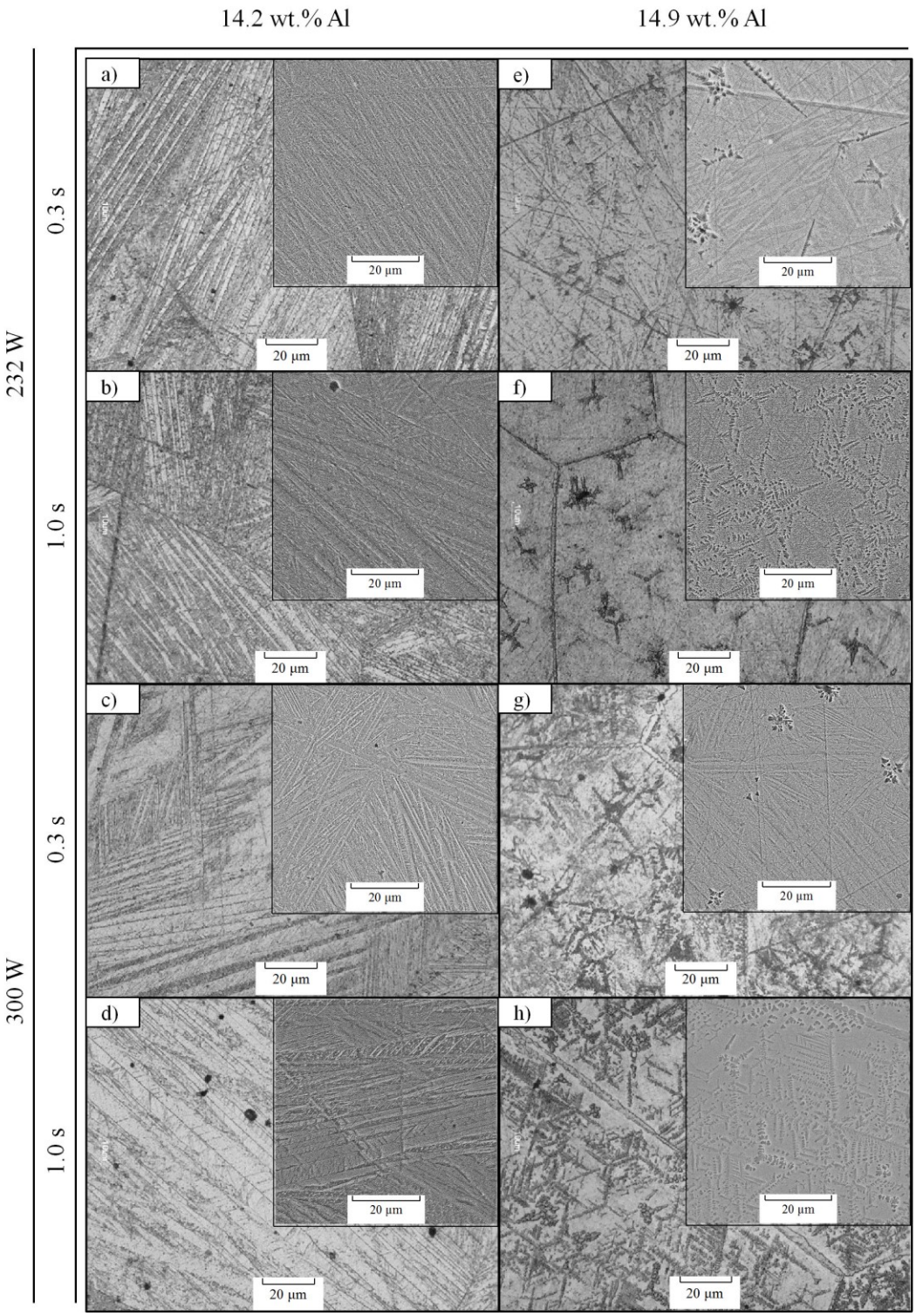

Fig. 7: Optical micrographs and SEM images (on the top of the right corner) of fabricated alloys.

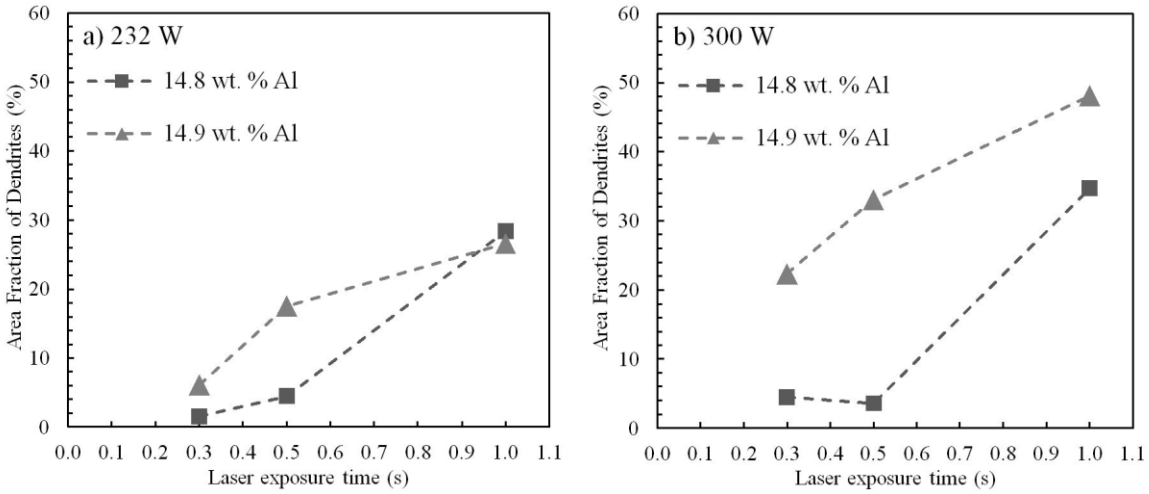

Fig. 8: Area fraction of dendrites in function of exposure time obtained (labeled at nominal composition) with laser power of: a) 232 W, and b) 300 W.

2.3.3. Transformation temperatures

All the alloys were found to undergo phase transformations in the temperature range 50°C – 240°C. Typical DSC analyses are shown in **Fig. 9**, whereas all the transformation temperatures and the associated transformation hysteresis obtained by estimating peak positions are summarized in **Fig. 10**. All the DCS curves show a well-shaped peak in the heating direction and another one in the cooling direction, separated by a constant difference of about 25°C. In general, both laser power and time of laser exposure affect the shape of the DCS curves with sharpest peaks observed for the shortest exposure times. Samples of higher Al content produce wider curves with lower transformation temperatures and higher transformation hysteresis. The temperature differences are more pronounced for samples with the lowest and highest wt.% Al, whereas small variation is observed between 14.8 wt.% and 14.9 wt.% Al. Further, samples with the highest Al content produce an additional peak of low amplitude, at about 0°C in the heating direction and, in some cases, a peak next to the principal one at high temperature, as shown in **Fig. 9**b. However, the additional peaks at about 0°C are not taken into account in this analysis.

The negative correlation of transformation temperatures and aluminum content as well as positive correlation with transformation hysteresis for all the samples is summarized in **Fig. 10**. No pronounced effect of laser power nor exposure time is observed.

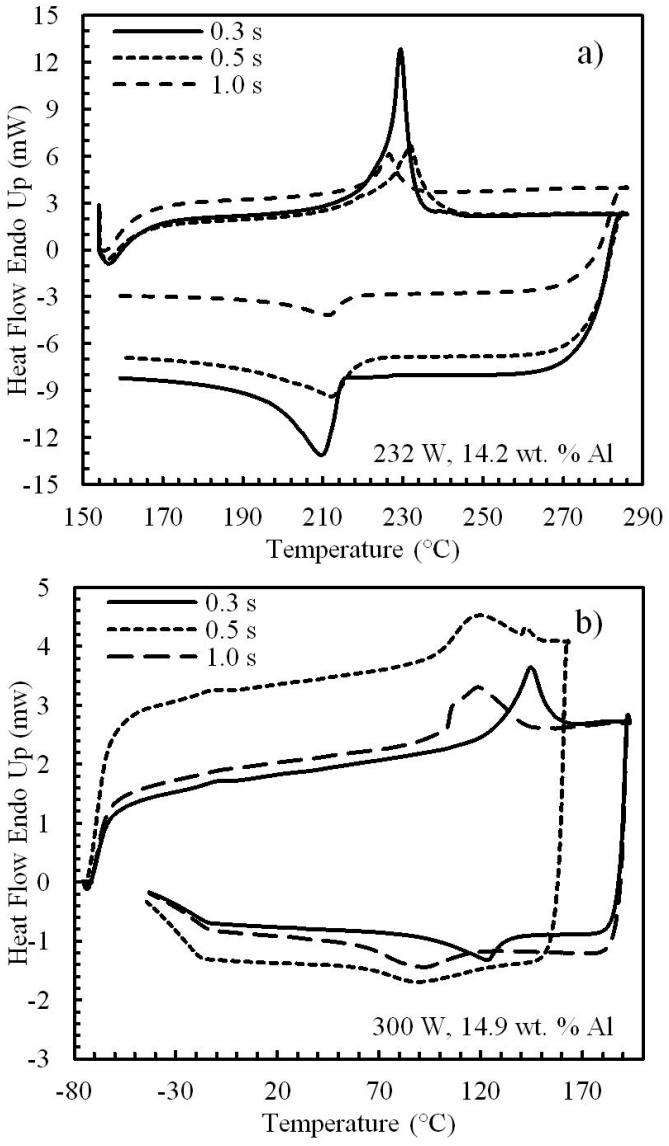

Fig. 9: DSC curves obtained for different laser exposure time on samples: a) 14.2 wt.% Al at 232 W (successful examples, narrow and high peaks typically observed by other authors in Cu-based shape memory alloys), and b) 14.9 wt.% Al at 300 W (examples exhibit potential secondary peaks).

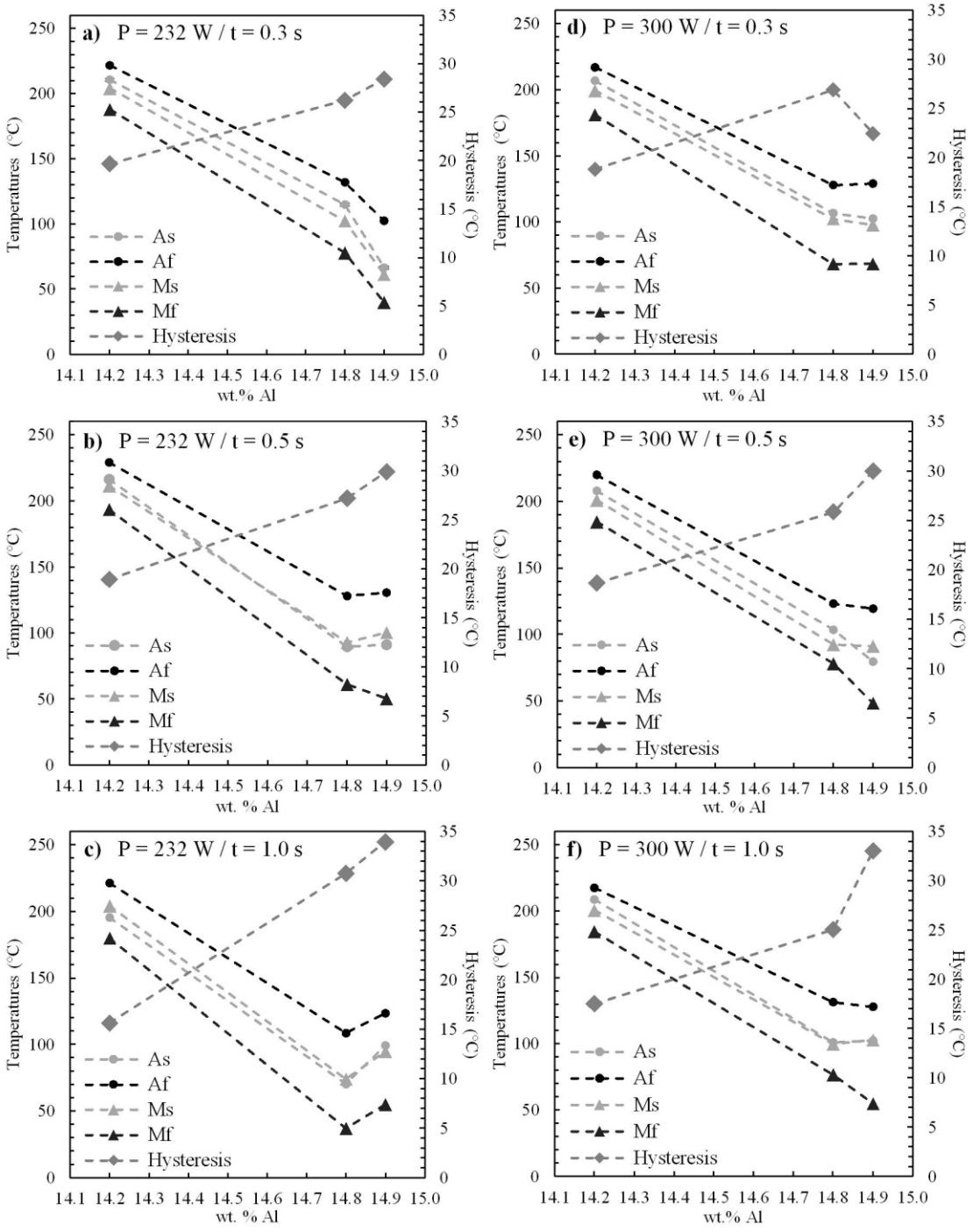

Fig. 10: Summary of the transformation temperatures (Martensitic start/finish temperatures: Ms/Mf; and Austenitic start/finish temperatures: As/Af) and hysteresis associated to those transformation temperatures, determined by DSC for samples fabricated with different processing parameters.

2.3.4. Hardness of the fabricated pieces

The microhardness measured on the polished samples are summarized in **Fig. 11**. Higher aluminum content correlates with higher values of hardness. A similar correlation is observed at higher laser exposure time, being more evident in the samples with high aluminum content. In spite of this, no significant effect of the laser power on the hardness was observed.

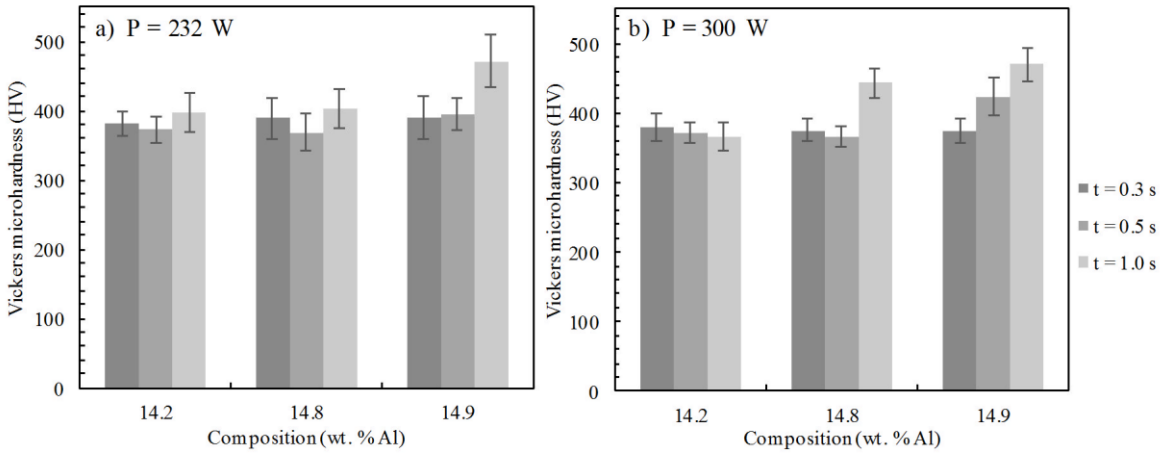

Fig. 11: Values of Vickers microhardness (HV0.2) obtained for all the alloys.

2.4. Discussion

Elemental composition of the obtained alloys deviate from the nominal values set by weighing the powders. In general, the relative content of Cu and Ni seem to have increased. The process of laser powder melting implies the transfer of a high power density in a short time, increasing the temperature locally above the melting point, and therefore an evaporation effect should be considered as a possible outcome. This has been studied by Verhaeghe et al. (2009) who proposed a model for selective laser melting with evaporation and concluded that evaporation is a phenomenon that cannot be neglected at realistic power inputs. The apparent evaporation of Al is likely due to its lower melting temperature and also possible considering the presence of impurities in

the initial powder. This explanation is supported by the observation of microstructures, which are of the same type for samples of nominal 14.8 and 14.9 wt% Al, but not correlated with the EDX data. In this regard. It is worth to note that the elemental composition obtained by the EDX technique has an error of the order of 1% due to the small analyzed area and the inhomogeneity in the fabricated pieces due to poor powder mixing.

Based on the microstructure analysis reported by Vajpai et al. (2013) and Recarte et al. (2002) the martensites with irregular zig-zag morphologies (**Fig. 7**b) and the ones with parallel plates changes (**Fig. 7**a) can be interpreted as β'_3 and γ'_3 phases. This observation implies that the obtained alloy has a SMA potential. On the other hand, considering the observations reported by Wang et al. (2011), the star-like dendrites observed in the specimens with 14.8 and 14.9 wt% Al (**Fig. 7**c, **Fig. 7**d, **Fig. 7**f and **Fig. 7**e) can be interpreted as γ_2 dendrite phases, which are very likely accompanied by (α+ γ_2). Also, the minute precipitations observed in the specimens fabricated with 14.2 wt% Al (**Fig. 7**a and **Fig. 7**b) can be interpreted as γ_2 phases (Guilemany & Fernhdez, 1995). It should be noted that an alloy with high aluminum content is more susceptible to precipitate γ_2 (Otsuka et al., 1999), whereas those precipitates do not contribute the shape memory effect and may even negatively affect the shape memory characteristics of the matrix. On the other hand, increasing the laser power or the time of laser application also increases the probability of producing γ_2 phases, which could be caused by a slower cooling rates due to a bigger mount of energy introduced into the system.

The previously observed changes in shape of the DSC curves by increasing laser power and time of laser exposure can be related to the increase of γ_2 precipitates which, in principle, hinder the transformation from austenite to martensite. As the increase of γ_2 precipitates are also sensitive to Al variations this will explain some similar changes in the shape of the DSC curves with an increase in Al content. However, an Al content increase also lowers the transformation temperatures. This variations in the transformation temperatures at variations of Al content are well known. Karagoz and Canbay (2013) concluded that Al content (wt.%) effects the reverse and forward transformation temperatures. On the other hand, Recarte et al. (2002) reported

something similar, and proposed an equation to estimate the martensitic temperature considering the Al and Ni content(wt.%).

The morphology of the martensites observed in **Fig. 7**a and **Fig. 7**b is indicative for the presence of β'_3 and γ'_3 martensites, however the values of hysteresis tends to increase with higher Al content (**Fig. 10**). Considering the observations of Recarte et al. (2002) and Vajpai et al. (2013) it is possible to assume that the low hysteresis (< 30°C) correspond with the $\beta_3 \Rightarrow \beta'_3$ transformation and a high hysteresis values (≥ 30°C) correspond with $\beta_3 \Rightarrow \beta'_3+\gamma'_3$ transformation. Therefore, the increase in the content of aluminum would not only increase the precipitation of γ_2 phases, but also produce an increase of the γ'_3 martensite formation. Similar to the γ_2 phase, the γ_3 is also not favorable for the shape memory properties of the material. The appearance of an additional peak in **Fig. 9**b in the curve at 0.5s of laser exposure is most probably associated with another phase, which is a common $\beta_3 \Rightarrow \beta'_3+\gamma'_3$ transformation. This can be correlated with the two close peaks observed in the DSC curve, corresponding to β'_3 peak the one at low temperature (Recarte et al., 2002). On the other hand, the hysteresis is more affected by the composition rather than laser parameters, which indicates that the martensite decomposition is more controlled by the composition of the alloy rather than the laser parameters.

The higher values of hardness found at higher Al content at long time of laser exposure should correspond to a combined effect of those parameter that causes an increase of γ_2 precipitates, which presents higher hardness values than the β'_3 phases reported by Wang et al. (2011). Moreover, it is well known that the Cu–Al–Ni crystals exhibit significant elastic anisotropy and for small indentations it could significantly influence the results. The differences between the measurements for specimens with the same composition are due to random analysis zones affected by the anisotropy of the alloy and by the probability to include (or not) γ_2 precipitates which exhibit higher hardness than β'_3 phases (Wang et al., 2011). Lojen et al. (2013) studied a Cu–Al–Ni alloy fabricated at different cooling rates with microharness indentation testing, finding some differences in the hardness depending on the grain direction and an important increase in the hardness when increasing the cooling rates (obtained an average of 320 HV for the

specimen with higher cooling rates). This suggests that in the experimental set-up used in the present work the cooling rates are not different enough to change the hardness of this alloy and the hardness of the specimens are mainly controlled by the dendrite growth of γ_2 phases precipitates in this case.

The set-up used in this study was shown sufficient for fabrication of Cu–Al–Ni alloys from elementary precursor powders but it is not yet suitable for producing larger specimens due to limitations of the available stepper motor. Preliminary tests to obtain a single line were performed with this experimental set-up presenting a discontinuous track made of several metallic balls. This behavior is known as the balling phenomenon. This consists in a diminishing in the surface energy of liquid reaching a final equilibrium state of several metallic agglomerates with spherical shape during laser melting along a row of powder particles (Gu, 2015). This is complex metallurgical phenomenon which presents at least three different working mechanism in some metallic alloys (Gu et al., 2007) and can be controlled by both powder material properties and the laser processing conditions (Gu, 2015). A better control over the resulting alloy composition could be obtained by improving the mixing process and the control of the evaporation rate by varying the gas pressure during the process (Masmoudi et al., 2015).

2.5. Conclusions

The results obtained in this study allow for the following conclusions:

1. Laser melting from powder mixture of elemental precursors permits the fabrication of Cu–based alloys with the characteristics of SMA.
2. Hysteresis of the phase transformations is determined mainly by the Al content.
3. The precipitation of γ_2 phase increases with the laser exposure time, laser power, and Al content.
4. The hardness values of the fabricated alloys are affected mainly by the precipitation of γ_2 phases. The pronounced increase of hardness at a combination of long laser exposure time at high power and higher Al content is associated with the formation of γ_2 dendrites.

BIBLIOGRAFIA

Abràmoff, M., Magalhães, P., & Ram, S. (2004). Image processing with imageJ. *Biophotonics International*, *11*(7), 36–41. http://doi.org/10.1117/1.3589100

Buehler, W. J., Gilfrich, J. V., & Wiley, R. C. (1963). Effect of Low-Temperature Phase Changes on the Mechanical Properties of Alloys near Composition TiNi. *Journal of Applied Physics*, *34*(5), 1475. http://doi.org/10.1063/1.1729603

Dagdelen, F., Gokhan, T., Aydogdu, A., Aydogdu, Y., & Adigu, O. (2003). Effects of thermal treatments on transformation behaviour in shape memory Cu – Al – Ni alloys, Mater Lett 2003; *57*(January), 1079–1085.

Deckard, C. R. (Austin T. (1989). Method and apparatus for producing parts by selectve sintering.

Delaey, L., & Chandrasekaran, M. (1994). Comments on “New description of long period stacking order structures of martensites in β-Phase alloys” by K.Otsuka, T.Ohba, M.Tokonami and C.M.Wayman. *Scripta Metallurgica et Materialia*, *30*(12), 1605–1610. http://doi.org/10.1016/0956-716X(94)90316-6

Gibson, I., Rosen, D. W., & Stucker, B. (2009). *Additive Manufacturing Technologies*. http://doi.org/10.1520/F2792-12A.2

Gu, D. (2015). *Laser Additive Manufacturing of High-Performance Materials*. Berlin, Heidelberg: Springer Berlin Heidelberg. http://doi.org/10.1007/978-3-662-46089-4

Gu, D., Meiners, W., Wissenbach, K., & Poprawe, R. (2012). Laser additive manufacturing of metallic components: materials, processes and mechanisms. *International Materials Reviews*, *57*(3), 133–164. http://doi.org/10.1179/1743280411Y.0000000014

Gu, D., & Shen, Y. (2007). Balling phenomena during direct laser sintering of multi-component Cu-based metal powder. *Journal of Alloys and Compounds*, *432*(1-2), 163–166. http://doi.org/10.1016/j.jallcom.2006.06.011

Gu, D., & Shen, Y. (2009). Balling phenomena in direct laser sintering of stainless steel powder: Metallurgical mechanisms and control methods. *Materials & Design*, *30*(8), 2903–2910. http://doi.org/10.1016/j.matdes.2009.01.013

Guilemany, J. M., & Fernhdez, J. (1995). Mechanism of two Way Shape Memory Effect Obtained by Stabilised Stress Induced Martensite, *5*(13).

Halani, P. R., & Shin, Y. C. (2011). In Situ Synthesis and Characterization of Shape Memory Alloy Nitinol by Laser Direct Deposition. *Metallurgical and Materials Transactions A*, *43*(2), 650–657. http://doi.org/10.1007/s11661-011-0890-x

Humbeeck, J. Van. (2001). Shape Memory Alloys: AMaterial and a Technology, (11), 837–850.

Jiao, Y. Q., Wen, Y. H., Li, N., He, J. Q., & Teng, J. (2010). Effect of solution treatment on damping capacity and shape memory effect of a CuAlMn alloy. *Journal of Alloys and Compounds*, *491*(1-2), 627–630. http://doi.org/10.1016/j.jallcom.2009.11.026

Karagoz, Z., & Canbay, C. A. (2013). Relationship between transformation temperatures and alloying elements in Cu–Al–Ni shape memory alloys. *Journal of Thermal Analysis and Calorimetry*, *114*(3), 1069–1074. http://doi.org/10.1007/s10973-013-3145-9

Kauffman, G., & Mayo, I. (1997). The Story of Nitinol: The Serendipitous Discovery of the Memory Metal and Its Applications. *The Chemical Educator*, *2*(2), 1–21. http://doi.org/10.1007/s00897970111a

Kruth, J. P., Froyen, L., Van Vaerenbergh, J., Mercelis, P., Rombouts, M., & Lauwers, B. (2004). Selective laser melting of iron-based powder. *Journal of Materials Processing Technology*, *149*(1-3), 616–622. http://doi.org/10.1016/j.jmatprotec.2003.11.051

Kyogoku, H., Ramos, J., Bourell, D. (2003). Laser melting of Ti-Ni shape memory alloy. *Proc SFF Symp, Austin, TX*, 668–675.

Liu, J. L., Huang, H. Y., & Xie, J. X. (2015). Superelastic anisotropy characteristics of columnar-grained Cu–Al–Mn shape memory alloys and its potential applications. *Materials & Design*, *85*, 211–220. http://doi.org/10.1016/j.matdes.2015.06.114

Lojen, G., Anžel, I., Kneissl, a., Križman, a., Unterweger, E., Kosec, B., & Bizjak, M. (2005). Microstructure of rapidly solidified Cu–Al–Ni shape memory alloy ribbons. *Journal of Materials Processing Technology*, *162-163*, 220–229. http://doi.org/10.1016/j.jmatprotec.2005.02.196

Lojen, G., Gojić, M., & Anžel, I. (2013). Continuously cast Cu-Al-Ni shape memory alloy - Properties in as-cast condition. *Journal of Alloys and Compounds*, *580*, 497–505. http://doi.org/10.1016/j.jallcom.2013.06.136

Masmoudi, A., Bolot, R., & Coddet, C. (2015). Investigation of the laser–powder–atmosphere interaction zone during the selective laser melting process. *Journal of Materials Processing Technology*, *225*, 122–132. http://doi.org/10.1016/j.jmatprotec.2015.05.008

Miyazaki, S., & Otsuka, K. (1989). Development of Shape Memory Alloys. *ISIJ International*, *29*(5), 353–377. Retrieved from https://www.jstage.jst.go.jp/article/isijinternational1989/29/5/29_5_353/_article

Mohd Jani, J., Leary, M., Subic, A., & Gibson, M. a. (2014). A review of shape memory alloy research, applications and opportunities. *Materials & Design*, *56*, 1078–1113. http://doi.org/10.1016/j.matdes.2013.11.084

Motoyasu, G., Kaneko, M., Soda, H., & McLean, a. (2001). Continuously cast Cu-Al-Ni shape memory wires with a unidirectional morphology. *Metallurgical and Materials Transactions A*, *32*(3), 585–593. http://doi.org/10.1007/s11661-001-0075-0

Ölander, A. (1932). An electrochemical investigation of solid cadmium-gold alloys. *Journal of the American Chemical Society*, *54*(10), 3819–3833. http://doi.org/10.1021/ja01349a004

Otsuka, K., & Wayman, C. M. (1999). *Shape Memory Materials*. Cambridge University Press. Retrieved from https://books.google.cl/books?id=DvItE9XUlN8C

Recarte, V., & Pérez-Sáez, R. (1997). Dilatometric study of the precipitation kinetics in Cu-Al-Ni shape memory alloys. *Le Journal de ...*, *7*(1 997). Retrieved from http://jp4.journaldephysique.org/articles/jp4/abs/1997/05/jp4199707C552/jp4199707C552.html

Recarte, V., Pérez-Sáez, R. B., San Juan, J., Bocanegra, E. H., & Nó, M. L. (2002). Influence of Al and Ni concentration on the Martensitic transformation in Cu-Al-Ni shape-memory alloys. *Metallurgical and Materials Transactions A*, *33*(8), 2581–2591. http://doi.org/10.1007/s11661-002-0379-8

Shishkovsky, I. V. (2005). Shape Memory Effect in Porous Volume NiTi Articles Fabricated by Selective Laser Sintering. *Technical Physics Letters*, *31*(3), 186. http://doi.org/10.1134/1.1894427

Sobrero, C., La Roca, P., Roatta, A., Bolmaro, R., & Malarría, J. (2012). Shape memory properties of highly textured Cu–Al–Ni–(Ti) alloys. *Materials Science and Engineering: A*, *536*, 207–215. http://doi.org/10.1016/j.msea.2011.12.104

Vajpai, S., Dube, R., & Sangal, S. (2013). Application of rapid solidification powder metallurgy processing to prepare Cu–Al–Ni high temperature shape memory alloy strips with high strength and high ductility. *Materials Science and Engineering: A*, *570*, 32–42. http://doi.org/10.1016/j.msea.2013.01.063

Van Humbeeck, J. (2001). 5.3 The Martensitic Transformation. *Materials Science Forum*, *366-368*(2001), 382–415. http://doi.org/10.4028/www.scientific.net/MSF.366-368.382

Van Humbeeck, J., Chandrasekaran, M., & Stalmans, R. (1993). Copper based shape memory alloys and the martensitic transformation. In *Proceedings of the International Conference on Martensitic Transformations* (pp. 1015–1025). Monterey, California, USA.

Verhaeghe, F., Craeghs, T., Heulens, J., & Pandelaers, L. (2009). A pragmatic model for selective laser melting with evaporation. *Acta Materialia*, *57*(20), 6006–6012. http://doi.org/10.1016/j.actamat.2009.08.027

Vernon, L., & Vernon, H. (1941). Producing molded articles such as dentures from thermoplastic synthetic resins. *US Pat*. Retrieved from http://scholar.google.com/scholar?hl=en&btnG=Search&q=intitle:Producing+Molded+Articles+such+as+Dentures+from+Thermoplastic+Synthetic+Resins#0\nhttp://scholar.google.com/scholar?hl=en&btnG=Search&q=intitle:Producing+molded+articles+such+as+dentures+from+t

Wang, Z., Liu, X. F., & Xie, J. X. (2011). Effects of solidification parameters on microstructure and mechanical properties of continuous columnar-grained Cu-Al-Ni alloy. *Progress in Natural Science: Materials International*, *21*(5), 368–374. http://doi.org/10.1016/S1002-0071(12)60071-9

Yuan, B., Zheng, P., Gao, Y., Zhu, M., & Dunand, D. C. (2015). Effect of directional solidification and porosity upon the superelasticity of Cu–Al–Ni shape-memory alloys. *Materials & Design*, *80*, 28–35. http://doi.org/10.1016/j.matdes.2015.05.001

A P E N D I X

A. INITIAL STATE OF THE METALIC POWDERS

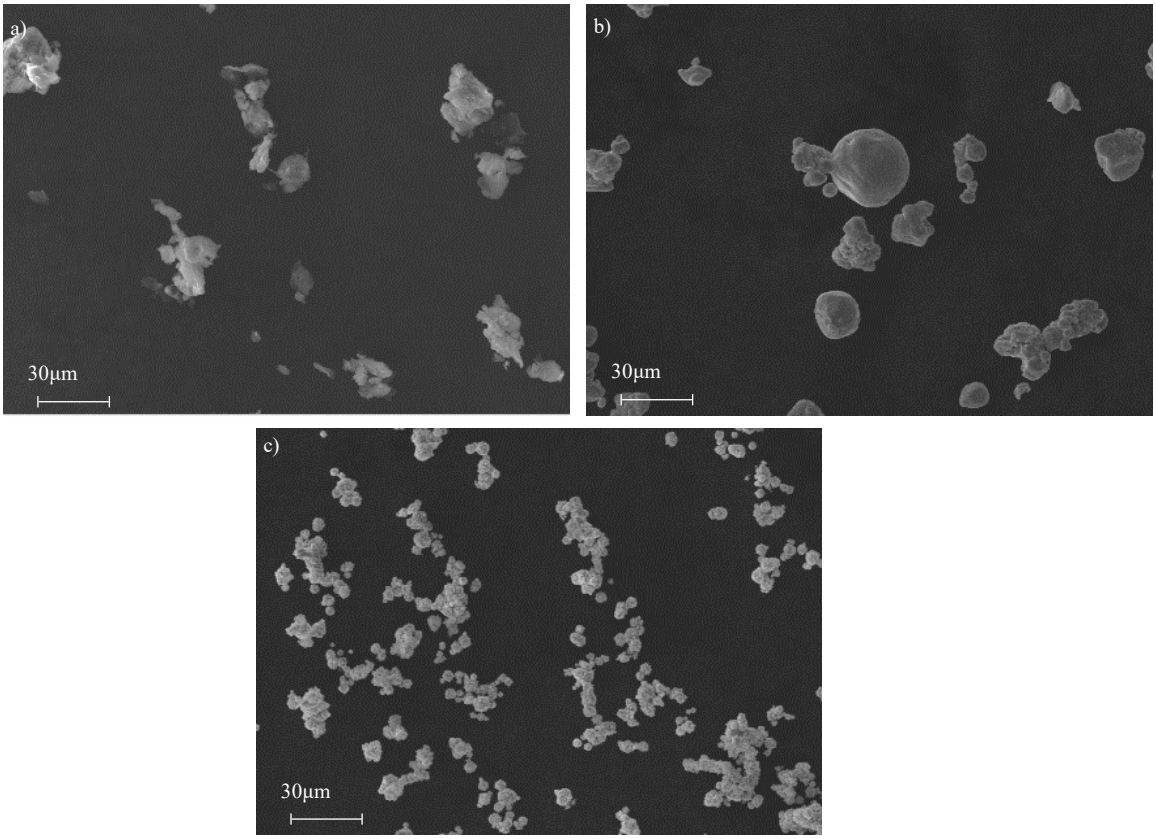

Fig. 12 SEM images (2500×) of the metallic elementary powders initial state: a) Al b) Cu and C) Ni.

Table 3: Weight composition of the elementary powders determined by EDX analysis

Elementary powder	Pure content (wt.%)	Oxygen content (wt.%)
Al	90.54	9.46
Cu	98.95	1.05
Ni	99.41	0.59

B. RESULTS

a. Detailed transformation temperatures

Here is presented in more detail the transformation temperatures (Austenitic start (A_s), austenitic finish (A_f), martensitic start (M_s), martensitic finish (M_f)) and transformation hysteresis (T_0) with their respective standard deviation (σ) obtained by the DSC measurements:

Table 4: Transformation temperatures and hysteresis of the fabricated specimens at 0.3 (s).

		t = 0.3 s									
P (W)	Wt.% Al	A_s	σA_s	A_f	σA_f	M_s	σM_s	M_f	σM_f	T_0	σT_0
232	14.2	210.7	13.3	221.6	10.1	203.9	9.5	187.9	8.3	19.7	1.9
	14.8	115.0	20.4	132.0	15.1	102.2	17.3	77.8	17.9	26.2	2.0
	14.9	66.6	32.7	102.4	9.9	61.4	25.2	40.0	25.5	28.4	2.1
300	14.2	206.7	11.3	216.8	10.9	199.1	6.4	180.8	6.9	18.8	2.8
	14.8	106.6	5.3	127.8	13.6	102.1	9.1	68.1	7.0	26.9	0.4
	14.9	102.3	42.7	129.0	36.3	97.7	36.0	68.3	42.3	22.4	12.2

Table 5: Transformation temperatures and hysteresis of the fabricated specimens at 0.5 (s)

		t = 0.5 s									
P (W)	Wt.% Al	A_s	σ A_s	A_f	σ A_f	M_s	σ M_s	M_f	σ M_f	T_0	σ T_0
232	14.2	216.4	7.1	229.0	6.3	211.3	6.2	193.4	5.8	18.9	2.1
	14.8	89.6	11.9	128.0	8.9	93.0	11.2	61.1	10.8	27.2	2.7
	14.9	91.2	15.7	130.5	4.7	100.4	14.7	50.4	10.5	29.9	5.3
300	14.2	207.9	17.1	219.8	14.5	200.8	14.7	184.5	11.3	18.7	2.6
	14.8	103.5	0.6	123.0	12.6	92.3	6.7	78.1	17.2	25.8	8.8
	14.9	79.5	17.6	119.5	17.5	91.2	22.6	48.4	16.2	30.0	2.1

Table 6: Transformation temperatures and hysteresis of the fabricated specimens at 1.0 (s)

		t = 1.0 s									
P (W)	Wt.% Al	A_s	σ A_s	A_f	σ A_f	M_s	σ M_s	M_f	σ M_f	T_0	σ T_0
232	14.2	195.4	25.6	221.3	13.4	204.0	13.5	179.9	19.0	15.6	0.9
	14.8	70.3	8.4	108.6	6.8	73.9	6.7	37.2	5.8	30.8	0.2
	14.9	99.2	5.2	123.5	16.8	94.6	15.1	55.0	10.9	33.9	7.7
300	14.2	208.6	5.1	217.4	6.5	200.6	5.6	184.4	6.4	17.5	1.1
	14.8	101.0	6.6	131.4	18.8	99.8	3.3	76.5	12.9	25.0	8.3
	14.9	102.4	0.3	127.8	22.2	102.8	16.8	54.9	10.6	33.0	7.2

b. Differential Scanning Calorimetry (DSC) curves

DSC curves obtained for different times of laser exposure at 0.3 (s), 0.5 (s) and 1.0 (s)

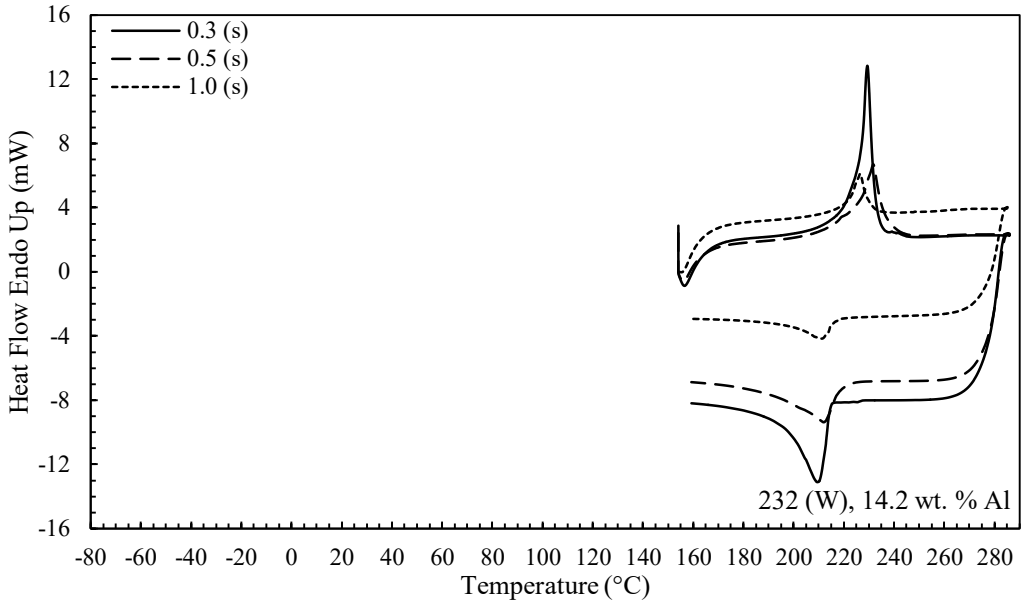

Fig. 13: DSC curves for 14.2 wt.% aluminum at 232 (W)

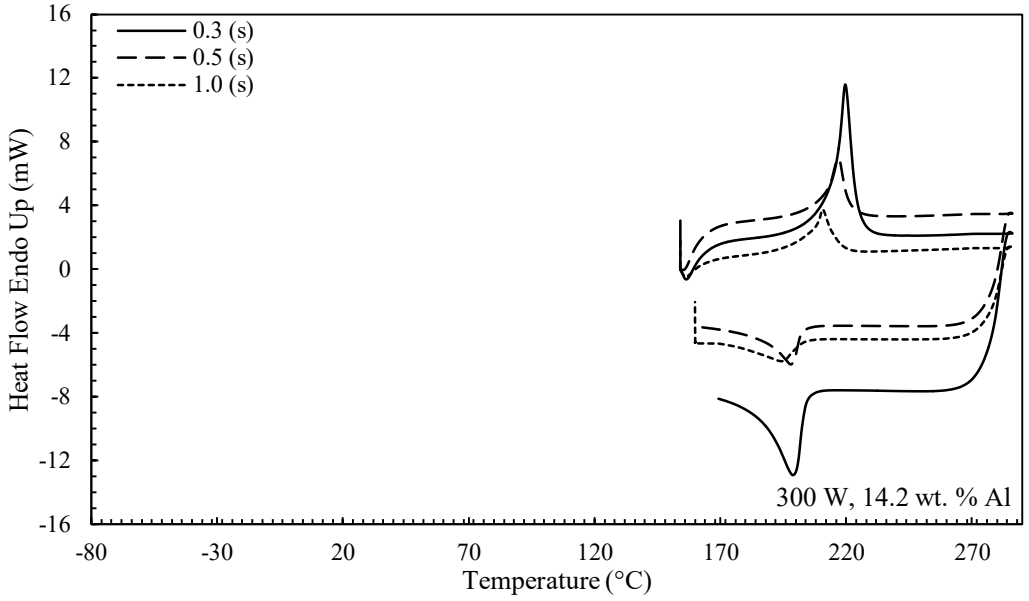

Fig. 14: DSC curves for 14.2 wt.% aluminum at 300 (W)

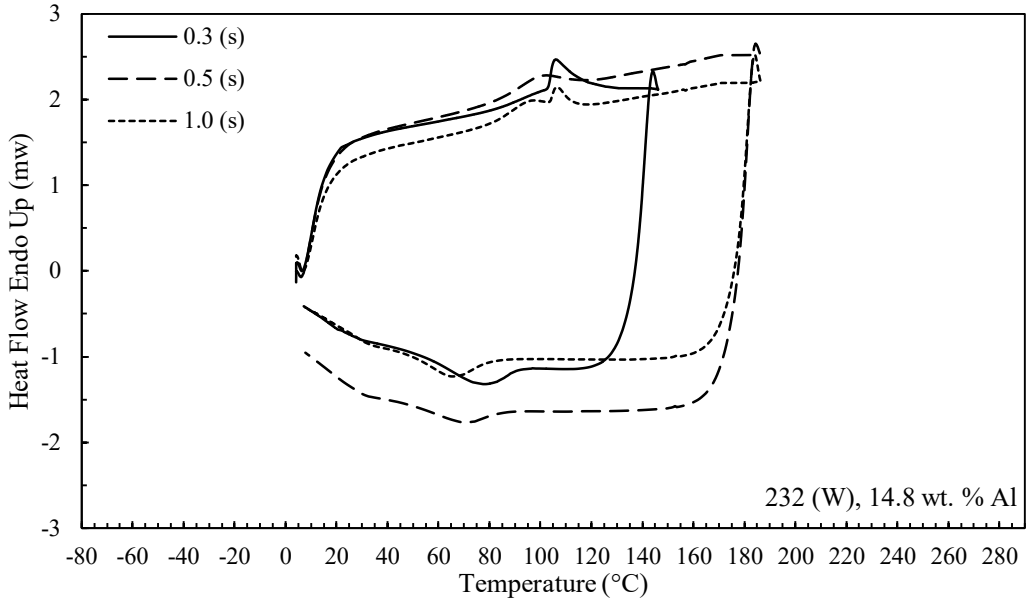

Fig. 15: DSC curves for 14.8 wt.% aluminum at 232 (W)

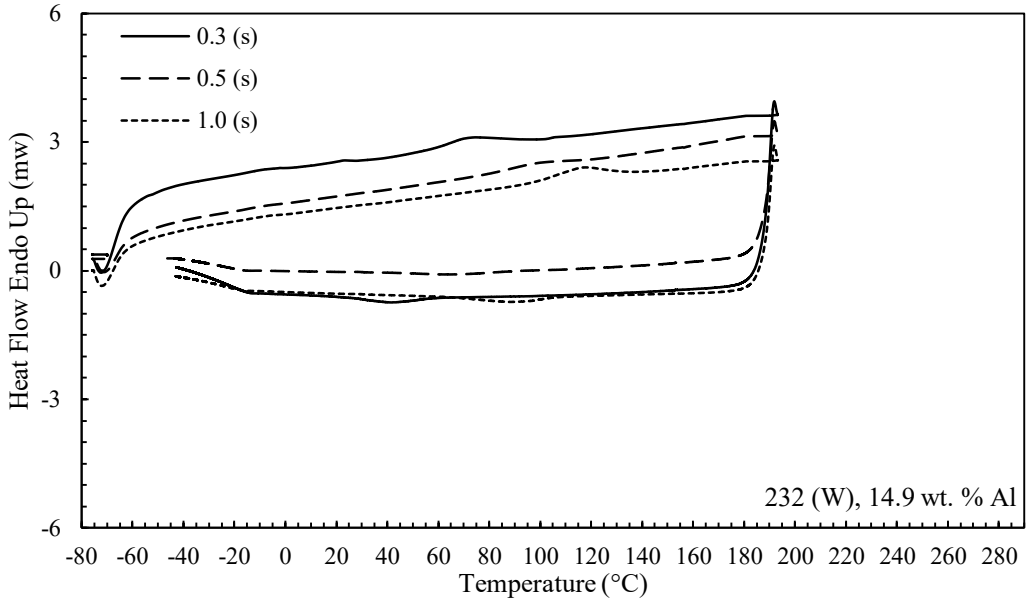

Fig. 16: DSC curves for 14.9 wt.% aluminum at 232 (W)

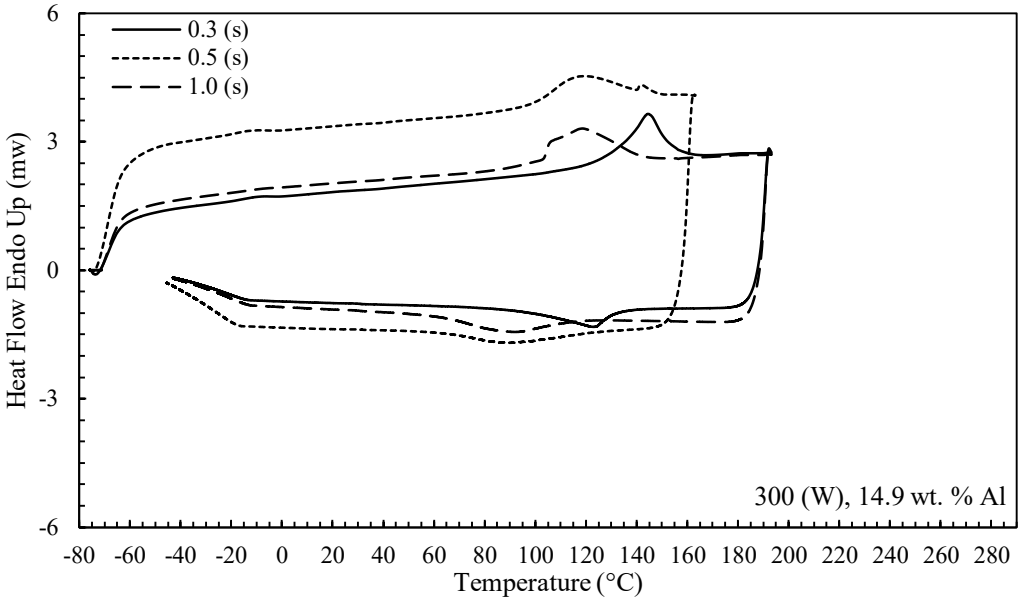

Fig. 17: DSC curves for 14.9 wt.% aluminum at 300 (W)

c. Hardness measurements

Table 7: Values of Vickers microhardness, HV0.2

N° Indentation	14.2SL	14.8SL	14.9SL	14.2ML	14.8ML	14.9ML	14.2LL	14.8LL	14.9LL
1	362.5	427	374	330	364.5	463.5	357	482	444.5
2	319	330.5	359.5	340.5	338.5	415	415.5	537.5	506
3	389	368	392.5	330	386.5	310	333.5	459	529
4	436	340.5	341	336	437	445.5	408.5	378	539.5
5	402	363	331	405.5	486	378	339	461.5	494.5
6	354	351.5	357	383.5	491	392	338	376	465
7	409.5	374	359.5	372.5	339	419	369.5	337	367
8	405	318.5	368	330.5	339	449	380.5	418	423
9	340.5	351.5	505.5	400	335.5	472	419	346	551
10	365.5	362	357.5	357	305	370	466	374	403.5
11	441	340.5	570	359.5	356.5	366	350	397.5	554
12	419.5	392	366	379	343	390	446	415	586
13	368	371	445	364	331	336	555.5	438	367
14	340.5	504	348.5	444.5	331	409.5	426.5	359.5	366
15	402.5	449	379.5	354	390	400	356.5	354	400
16	354	466.5	339	449	363	384.5	389	349	453

17	377	494.5	419	399	325.5	319.5	409	370	558
Average	381.5	388.5	389.0	372.6	368.4	395.3	397.6	403.1	471.0
Standard Deviation	35.2	57.9	63.9	37.3	54.5	47.2	56.8	56.2	74.8

Table 8: Values of Vickers microhardness, HV0.2 (Continuation)

N° Indentation	**14.2SH**	**14.8SH**	**14.9SH**	**14.2MH**	**14.8MH**	**14.9MH**	**14.2LH**	**14.8LH**	**14.9LH**
1	414	466	374.5	382	426.5	390	308	393.5	541.5
2	409	380.5	383.5	323.5	365.5	415.5	359.5	432.5	581.5
3	408.5	385	383.5	368	354	395	354	519.5	486
4	445	374.5	365.5	383.5	316.5	352	415.5	469	457
5	376.5	365	351	362.5	368.5	415.5	354	412	515.5
6	343	346	359.5	438.5	354.5	372.5	316.5	467.5	445
7	343	354.5	454.5	366.5	360.5	374.5	381.5	449.5	449.5
8	354	377	351.5	343.5	309.5	482	366	457.5	437.5
9	421	343.5	363.5	349	348.5	423	390.5	465.5	445
10	281.5	361	405.5	376.5	389.5	457	377	402	533.5
11	367.5	335.5	339	406.5	346	374.5	371.5	389	534
12	437.5	363.5	342	360	346	393.5	311.5	387	442
13	362.5	400	338	402	365	457	351.5	412.5	495.5

14	371.5	389.5	401.5	405	415.5	509	351.5	419	434
15	367	385	435	386	371.5	489	492.5	481.5	430.5
16	362.5	406.5	365.5	341.5	397.5	366.5	363	518	486
17	377	338.5	341.5	326	383.5	523.5	359.5	457	398.5
Average	378.9	374.8	373.8	371.8	365.8	422.9	366.1	443.1	477.2
Standard Deviation	40.4	31.5	33.8	30.7	30.7	53.6	42.6	41.8	49.8